K and Au Bicatalyst Assisted Growth of Carbon Nanocoils from Acetylene: Effect of Deposition Parameters on Field Emission Properties

Tsung-Yu Tsou,[†] Chi-Young Lee,[‡] and Hsin-Tien Chiu*,[†]

[†]Department of Applied Chemistry, National Chiao Tung University, Hsinchu, Taiwan, 30050, R. O. C.
[‡]Department of Materials Science and Engineering, National Tsing Hua University, Hsinchu, Taiwan, 30043, R. O. C.

S *Supporting Information*

ABSTRACT: We demonstrated the growth of carbon nano-coils (CNCs) via chemical vapor deposition (CVD) using Au and K metals as the catalysts to assist the thermal decomposition of C_2H_2. Typical CNCs (wire diameter: 50–80 nm, coil diameter: 110–140 nm, pitch: 100–200 nm, tens of micrometers), identified as amorphous coiled carbon fibers by scanning electron microscopy (SEM) and transmission electron microscopy (TEM), were grown at proper combinations of reaction parameters. Au nanoparticles (NPs), identified by energy dispersion X-ray spectroscopy (EDX) and electron diffraction (ED), were located at the tips of the CNCs. The observations suggested that a tip-growth mechanism involving the Au NPs as the nucleation sites was in operation. In the reaction, the liquid-phase K metal assisted the decomposition of C_2H_2 by lowering the reaction temperature. We propose that acetylide and hydride intermediates were formed in the reaction. Further decomposition of the acetylide intermediates generated solid-phase carbon to grow the CNCs. Effects of varying the reaction conditions on the CNC growth were investigated. On the basis of the results, a Au and K bicatalyst enhanced tip-growth vapor−liquid−solid (VLS) mechanism was proposed to rationalize the CNC formation process. Electron field emission (EFE) characteristics of the CNCs were studied. The best EFE result showed a turn-on field (E_{to}) of 3.78 V/μm and a field enhancement factor (β) of 1852. In addition, the current density (J) was as high as 43 mA/cm^2 at 6.87 V/μm. The data suggest that the CNCs could be employed for field emission device applications.

KEYWORDS: *carbon nanocoils, Au catalyst, K catalyst, field emission*
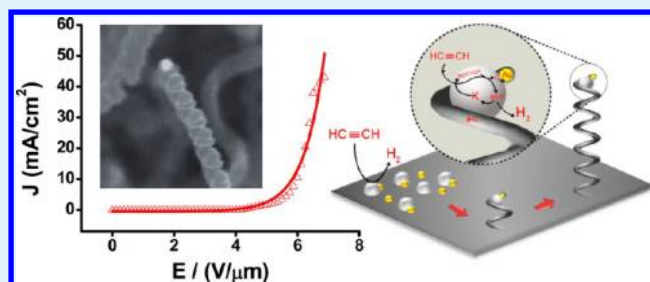
INTRODUCTION

Various carbon nanomaterials, including carbon nanotubes (CNTs), carbon nanofibers (CNFs), carbon nanocoils (CNCs), and fullerenes, have been intensively investigated because of their intrinsic properties such as chemical stability, high mechanical strength, high external surface area, and good thermal and electrical conductivity.[1−5] They are used in a wide range of applications, including semiconductor devices, field emission devices, biomedical components, catalysis, electrochemical electrodes, and analysis.[6−19] Among these nanostructures, CNCs are expected to have special properties and possible unique applications because of their three-dimensional (3-D) helical morphologies. Several synthetic methods have been reported to fabricate CNCs. These include chemical vapor deposition (CVD), arc-discharge, flame synthesis, and hydrothermal synthesis.[13,20−22] Among them, CVD is the most widely used one. Many groups have employed CVD to grow CNCs via catalytic decomposition of hydrocarbons, employing many different metal catalysts.[23−28] Even though several growth mechanisms have been proposed to rationalize CNC growths, new pathways are still possible.[29−32] Recently, we observed growth of CNCs by thermal decomposition of C_2H_2 on Si substrates through a novel Ag and K bicatalyst assisted vapor−liquid−solid (VLS) tip-growth route.[13] We suggest that K assisted the decomposition of C_2H_2 by forming relatively stable acetylide and hydride intermediates, while Ag nanoparticles (NPs) acted as the tips for the CNC growths. In addition, we propose that the affinities between the liquid-phase K and the as-deposited solid C caused the growing one-dimensional material to curl into coils. To explore other possible cases operated via this route and to seek better control of the CNCs' uniformity, we report here the use of Au NPs and K as the bicatalysts to assist the thermal decomposition of C_2H_2 on flexible graphite foils. The graphite substrates offer higher conductivity, lower cost than Si, and more potential to integrate CNCs into bendable electronic devices.

With proper control of the reaction parameters, uniformly shaped CNCs on the graphite substrates can be employed for electron field emission (EFE) applications. EFE is a quantum tunneling process which extracts the electron from the material

surface into the vacuum level by applying a sufficient external electric field.[33] The performance is sensitive to the composition, morphology, and aspect ratio of the emitting material. Among many potential materials, C-based emitters are widely explored due to their excellent physical and chemical properties.[2−5,34−41] Because of their unique morphology, CNCs have shown excellent EFE characteristics.[42,43] In this article, we wish to report our investigations on the factors affecting the growth of CNCs and the variables influencing their EFE properties.

■ EXPERIMENTAL SECTION

Materials. Graphite foils (Alfa Aesar 99.8%, thickness: 0.5 mm) were used as the substrates. A Au target (99.99%) in a direct current (DC) sputtering system provided the source for the deposition of Au NPs on the substrates. KH powders (Sigma Aldrich, 30 wt % dispersion in mineral oil) were washed with anhydrous hexane and dried under an inert atmosphere prior to use. Locally supplied gases, C_2H_2 (99.5%), H_2 (99.9999%), and Ar (99.9999%), were used in the reactions without further purification.

Growth of CNCs. The growth of a representative CNC sample, sample **22** listed in Table S1 in the Supporting Information, is described below. The graphite foil was first cleaned with alcohol and acetone. A thin layer of Au was deposited on the substrate by DC sputtering (2.2 kV, 30−35 mA, background pressure 7×10^{-2} mbar) for 20 s. Then, it was placed in a quartz boat (length: 10 cm) and loaded into a quartz tube inside a tube furnace (Lindberg Blue M, heated length: 61 cm). The boat was placed at 25 cm downstream from the center of the furnace. The system was evacuated and filled with Ar several times to ensure an air-free reaction environment. Another quartz boat (length: 10 cm) loaded with KH powders (0.18 g) was placed at the center of the furnace under continuous Ar purge. Then, KH was thermally decomposed at 623 K (ramping rate 10 K min^{-1}) in Ar for 1 h and cooled to 423 K gradually. After the reactor was evacuated below 10^{-3} mbar, K was evaporated at 423 K to deposit a thin layer of K film on the substrate for 20 min. During the K deposition, the temperature at the substrate was 353−373 K. Then, under continuous Ar purge, the quartz boat loaded with the K- and Au-coated graphite substrate in the quartz tube was pulled to the center of the furnace. Then, at 723 K, $C_2H_{2(g)}$ (2.7 sccm) and $H_{2(g)}$ (20 sccm) were passed over the substrate for 1 h. Growth of a black thin film on the substrate was observed. After the substrate was cooled to room temperature under Ar, K-containing byproducts were removed by deionized (DI) water. Finally, the product was dried in air before further characterizations. The growth parameters of other samples were listed in Table S1 in the Supporting Information also.

Instruments. Morphologies and compositions of the samples were characterized using field emission scanning electron microscopes (FESEM, Hitachi S-4000, Hitachi S-4700, and JEOL 7401F, at an accelerating voltage of 15 KeV) equipped with energy dispersive X-ray (EDX) systems. The crystallinity and microstructural details were studied using JEOL JSM-2010 (200 kV) and JEOL JEM-3000F (300 kV) high-resolution transmission electron microscopes (HRTEM).

Electrical Field Emission Measurements. EFE measurements were investigated using a homemade instrument. The high vacuum (2.5×10^{-6} mbar) testing system was equipped with an oil-free turbo-molecular pump (Alcatel ATP400C) and a rod-shaped tungsten anode (tip diameter: 2 mm) attached to an X−Y−Z manipulator. The EFE properties were determined using a simple diode configuration with the substrate fixed on the sample stage as the cathode. The distance between the tip and the sample was adjusted by a micrometer on the manipulator. The emission currents were measured with a Keithley 2410 which also acted as the power supply (0−1100 V, with an increment of 20 V).

■ RESULTS AND DISCUSSION

SEM Characterizations. CNCs were grown on graphite substrates via CVD using Au and K metals as the catalysts. As

discussed below, the metals act cooperatively to assist the thermal decomposition of C_2H_2 and the coil growths. A summary of the samples grown at various combinations of reaction conditions is shown in Table S1 in the Supporting Information. Analyses of a representative sample, **22**, are described below as an example. In Figure 1, SEM images and an
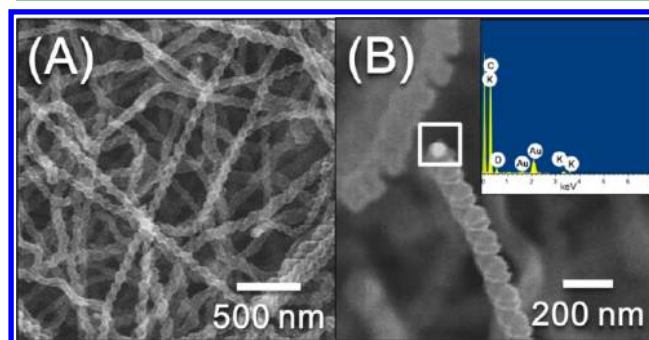

Figure 1. SEM images of as-grown CNCs in sample **22**. (A) Low- and (B) high-magnification top-view images. Inset: EDX from squared region.

EDX spectrum of **22** are shown. Figure 1A displays the presence of a high density of CNCs on the graphite substrate. In Figure 1B, a NP located at the tip of a CNC can be observed. An EDX analysis from the squared region in Figure 1B shows the signals of C, Au, K, and O. The K and O atoms can be removed by washing in DI water and are assigned to oxidized forms of K located mainly on the CNCs. The wire diameter, coil diameter, and pitch of the CNCs are determined to be 46−88, 77−109, and 59−127 nm, respectively. Since the CNCs are entangled, their lengths are difficult to measure. From the thickness of the CNC layer on the substrate, we estimate that the coil lengths can be more than 10 μm.

TEM Studies. To further characterize **22**, TEM investigations were carried out. The results are shown in Figures 2 and 3. Figure 2A shows the image of a CNC, with a coil diameter of 100 nm and a pitch of 100 nm. A high-magnification image in Figure 2B, from the squared region in Figure 2A, illustrates that the coil has a wire structure with a diameter of 40−50 nm. An HRTEM image in Figure 2C and a selected area electron diffraction (SAED) pattern in Figure 2D, also from the squared region, reveal that the coil body is amorphous. Figure 3 shows the data from another CNC. As shown in Figure 3A, the coil diameter is estimated to be 100 nm. In addition, a particle can be seen at the tip. An EDX spectrum of the particle, shown in Figure 3B, suggests that the particle contains Au mainly, and no signals from K are found. This agrees with the assumption that the oxidized forms of K were fully removed during the TEM sample preparation. The Cu signal is attributed to the Cu grid which held the sample. Figure 3C is the HRTEM image of the particle. From the image, a fringe spaced at 0.23 nm could be assigned to the lattice spacing of (111) planes of face-centered cubic (fcc) Au (JCPDS 89-3697). The SAED pattern in Figure 3D shows a single crystalline pattern from (11−1), (111), and (002) planes of fcc Au observed from the [−110] zone axis. Two sets of diffused ring patterns are also observed. They are assigned to the less ordered CNC structure.

Effect of Reaction Conditions on CNC Growths. A series of experiments with varied reaction conditions, as summarized in Table S1 in the Supporting Information, were
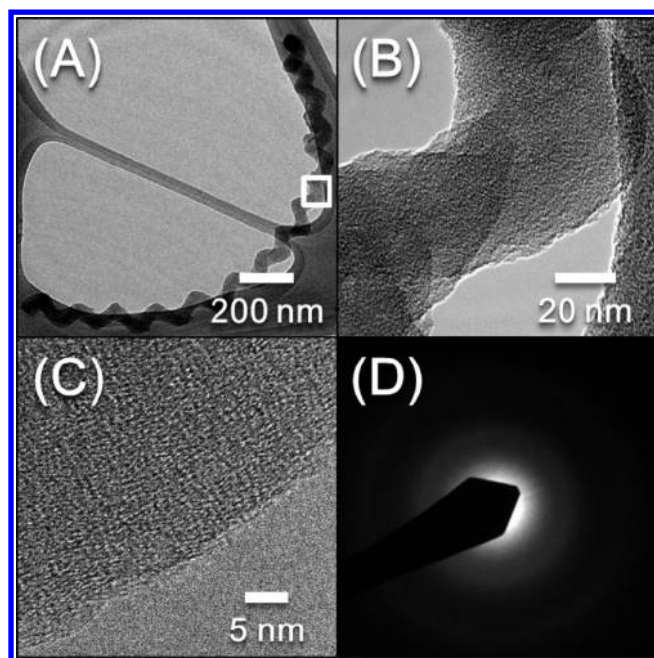
Figure 2. TEM studies of a CNC in sample **22**. (A) Low-magnification image. (B) High-magnification, (C) high-resolution, and (D) SAED pattern from the squared region in (A).
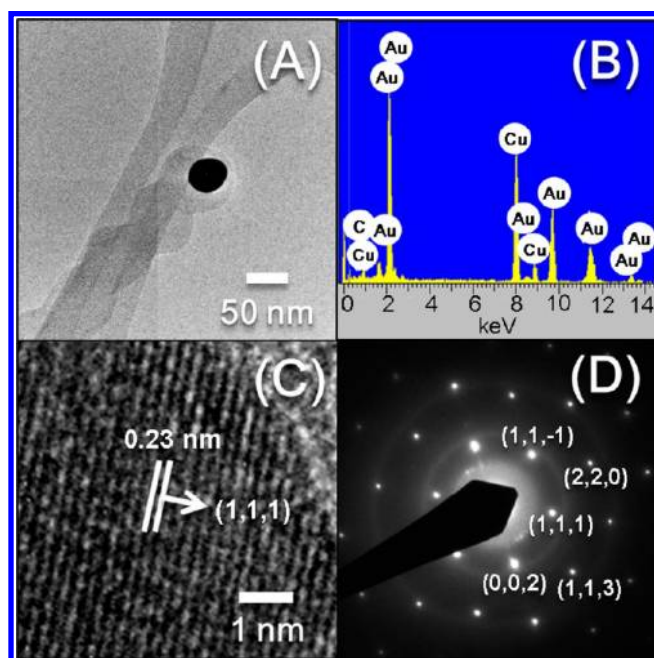

Figure 3. TEM studies of a CNC in sample **22**. (A) Low-magnification image showing a NP at the tip. (B) EDX from the tip. (C) High-resolution image and (D) SAED pattern of the NP. The Cu signals in (B) are assigned to the TEM grid.

performed. The results suggest that the growth conditions affected the final products greatly. How these variables affected the morphology and property of the CNCs will be discussed below.

Figure S1 (Supporting Information) shows the effects of sizes of Au NPs (deposited by varying the sputtering time) and coating time of K metal on the C growths performed at 723 K. In Figure S1 (Supporting Information), A1−D1 display the SEM images of graphite substrates decorated with Au NPs

before the C depositions. Without the presence of K, no C nanostructures can be grown on these substrates (samples **5−8**, images A2−D2 in Figure S1 (Supporting Information), correspondingly). On the other hand, in the reactions with just K on the substrates, only featureless C layers were obtained (images not shown). In contrast, in experiments with both Au and K deposited on the substrates, we observe the growths of C nanostructures in the forms of NPs, nanowires (NWs), and NCs (samples **1−4** and **9−12**, images A3−D3 and A4−D4 in Figure S1 (Supporting Information), respectively). It has been known that both Na and K can function as dehydrogenation catalysts to assist the deposition of C from C_2H_2.[13,44] The images confirm the role of Au NPs as the nucleation seeds for the one-dimensional (1D) nanostructure formation again. Figure S2 in the Supporting Information shows size distribution histograms of the sputtered Au NPs on the substrates prior to the growths of **1−4**. As the sputtering time is increased from 15 to 50 s, the average size of Au NPs increases from 30 ± 9 to 63 ± 21 nm. After the deposition of K on these substrates, NCs and curled NWs were obtained, as shown in Figure S3 in the Supporting Information for samples **1−4**. Clearly, as the Au NP diameter increases, the NC and the NW diameters are increased as well. In general, CNCs were grown from smaller Au NPs (averaged size 30−39 nm), while curved NWs were the result of large Au NPs (average size 63 nm). Side-viewed C layer images (Figure S3C, F, I, and L, Supporting Information) also indicate that the density of the 1D products increases with the increasing density of Au NPs. Figure 4 summarizes the effect of the Au NP sizes on the CNC dimensions (wire diameter, coil diameter, and pitch). All of the results suggest that they are proportional to the Au NP sizes. The role of the Au NPs is supported further by the SEM images displayed in Figure 5. They reveal the nanostructures grown for only 2 min. For each individual nanostructure, a NP wrapped inside a curved 1D carbon fiber can be seen. On the basis of the data, the CNCs probably are grown via a NP assisted tip-growth mechanism.

To determine a proper carrier gas composition for CNC formation, the following conditions were attempted for experiments carried out at 723 K: H_2 20 sccm, H_2 30 sccm, and Ar 20 sccm. SEM images of samples **2**, **13**, and **14** are displayed in Figure S4 (Supporting Information), respectively. Clearly, when H_2 20 sccm was used, CNCs were formed in **2** (Figure S4A−C, Supporting Information). As shown in Figure S4D−F (Supporting Information), in the experiment using a high H_2 flow rate of 30 sccm, not only the nanostructure density decreases but also the morphology changes to worm-like NWs in **13**. The above observations suggest that in an H_2-rich atmosphere more K surface sites are occupied by H atoms. This not only decreases the catalytic activity of K metal but also decreases the adhesion between the deposited C and the liquid surface of K. When Ar was used, only micrometer-sized C particles were obtained for **14** (Figure S4G−I, Supporting Information). We propose that in this H_2-poor environment H atoms on the K surface associate into H_2 and desorb easily. This generates a H-poor K surface which can be covered by C atoms fully to form featureless C particles displayed in Figure S4G−I (Supporting Information).

To find proper CNC deposition rates, the reaction temperatures 673−773 K were attempted. Figure S5 (Supporting Information) displays the morphologies of the C materials deposited in the experiments. Clearly, CNCs could not grow at 673 K in sample **15** (Figure S5A, Supporting Information),
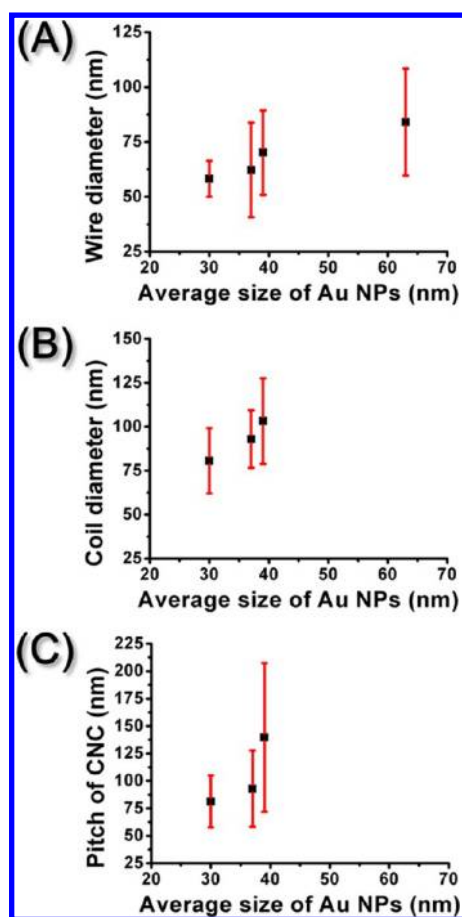
Figure 4. Variation of CNC structural parameters in samples **1**−**4**. (A) Wire diameters, (B) coil diameters, and (C) coil pitches against average Au NP sizes.
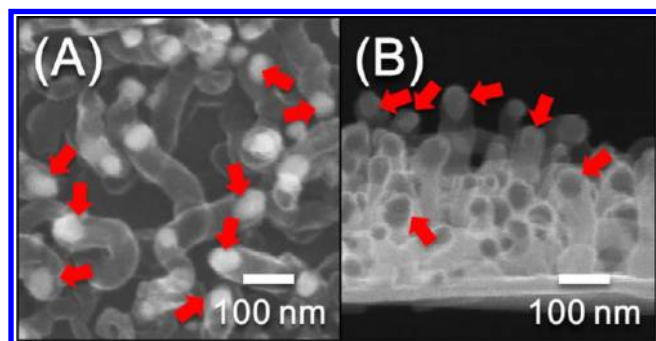

Figure 5. SEM images of C segments grown on the substrate for 2 min. (A) Top and (B) side views. Arrows indicate examples of Au NPs wrapped inside the tips of elongating C segments.

while at 773 K, sample **16**, a C film, was obtained (Figure S5B, Supporting Information). Obviously, at low temperatures, the overall growth rate was too low to offer CNCs. On the other hand, at high temperatures, the decomposition of C_2H_2 was too fast to grow 1D products. Instead, a C film was deposited rapidly. The observations suggest that the reaction temperature influences the growth rate and the final morphology significantly. Only at 723 K, as shown in Figure S5C and D (Supporting Information), CNCs are found in sample **2**. Thus, the temperature was selected as the optimized growth temperature for CNCs throughout this study.

After the proper carrier gas flow rate and the reaction temperature were selected, the effect of C_2H_2 flow rate on CNC morphology was examined. Figure S6 (Supporting Information) shows the CNCs (samples **2** and **17**−**19**) grown at C_2H_2 flow rates of 2.7−22 sccm and 723 K for 20 min. The results are summarized in Table S2 in the Supporting Information. Using the data, the effect of the flow rate on the CNC diameter and layer thickness are plotted in Figure 6. As
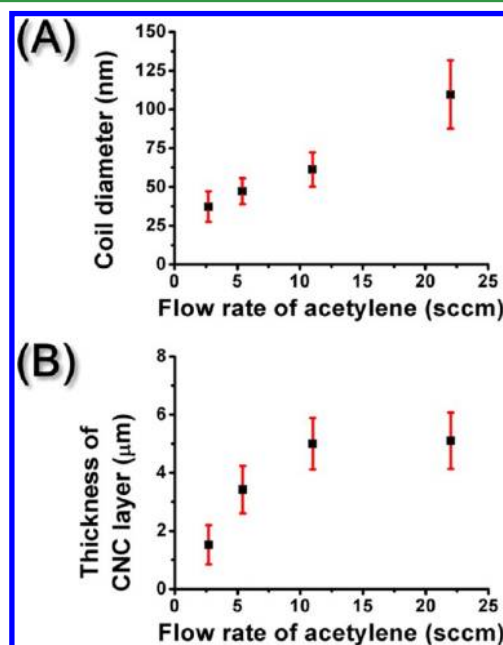

Figure 6. Variation of CNC (A) coil diameters and (B) layer thicknesses in samples **2** and **17**−**19** against C_2H_2 flow rates.

the flow rate of C_2H_2 is increased from 2.7 to 22 sccm, the coil diameter increases from 37 nm for **2** to 110 nm for **19**. The coil pitch does not change much. In addition, as the flow rate is increased from 2.7 to 11 sccm, the CNC layer thickens from 1.5 μm for **2** to 5.0 μm for **18**. Although the layer thickness of **19** does not increase much at 22 sccm, its coil diameter widens significantly at this condition. In general, the amount of deposited C increases proportionally to the increased C_2H_2 flow rate. The results indicate that a high flow rate of C_2H_2 leads to a high concentration of the reactant near the reaction sites. Consequently, on the catalyst surface, the growth rate is enhanced, resulting in the increased coil diameter and the CNC layer thickness.

Figure S7 in the Supporting Information shows the SEM images of the CNCs **18**, **20**, and **21** grown at a C_2H_2 flow rate of 11 sccm and 723 K for 20−180 min. Using the morphological data displayed in the images, the averaged CNC diameters and layer thicknesses are summarized in Table S3 (Supporting Information) and plotted in Figure 7. It is reasonable to find that the CNC layer thickness increases proportionally with the increasing growth time because the tip-growth mechanism was in operation. Interestingly, the CNC diameters also increase with the increasing time. Probably, due to the good adhesion between C and liquid-phase K, the residual metal on the C surface assisted further dehydrogenation of C_2H_2 to deposit more C and widen the fiber diameters.

Proposed Growth Mechanism. Although several Au-based catalytic systems have been shown to assist CNT growths and several CNC growth mechanisms have been proposed,
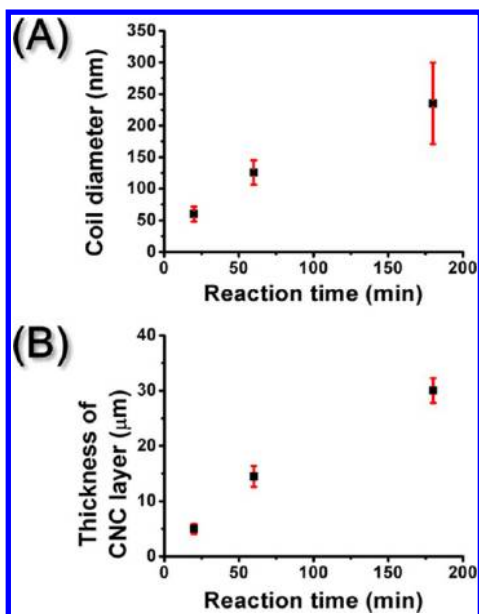
Figure 7. Variation of CNC (A) coil diameters and (B) layer thicknesses in samples **18**, **20**, and **21** against reaction time lengths.

they could not be applied to our study because the reaction conditions were very different.[26,31,45−48] Thus, based on the data presented above and the mechanism proposed in our previous report, a reaction pathway is presented in Scheme 1 to

Scheme 1. Proposed Growth Pathway of CNC on Graphite Foil
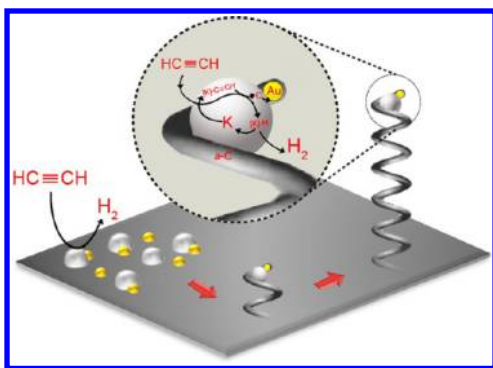
rationalize the CNC growth process.[13] The presence of both Au and K metals in the reaction is the most important factor for the CNC formation. As supported by the experimental data, the presence of fine crystalline Au NPs at the tips of CNCs reveals that Au and K do not form alloys under the reaction conditions. Our investigations indicate that without the Au NPs the CNCs would not grow. This is a strong indication that a VLS process is in operation. K metal also plays a critical role in the reaction. Without it, C_2H_2 does not decompose at the temperatures employed in this investigation. The liquid-phase metal acts as not only a C_2H_2 dehydrogenation catalyst to assist the carbon deposition but also a soft template to shape the coil formation.[13] As suggested in Scheme 1, K metal assists the C−H bond dissociation and converts C_2H_2 into relatively stable acetylide and hydride. Further decomposition of the intermediates leaves C atoms to nucleate at the Au NP and elongate into a 1-D fiber. It is expected that a relatively good adhesion exists between the liquid-phase K and the solid C.

Consequently, the C deposition rate at the C−K interface, which is located at the inner curvature of the coil, could be slower than that at the exposed surface, the outer curvature. This may influence the NW curling also. As shown in the scheme, after the hydride decomposes, H_2 desorbs from the surface, and the K catalyst is regenerated.

Effect of Reaction Conditions on Electron Field Emission Properties of CNCs. To examine the effectiveness of the CNCs as electron field emitters, measurements of their performances were carried out. The experimental data were further analyzed by using the Fowler−Nordheim (FN) theory which predicts that total emission current J as

$$J = A(\beta^2 E^2/\phi)\exp(-B\phi^{3/2}/\beta E)$$

Here, ϕ is the work function, assumed to be 5 eV, and β is the field enhancement factor, determined by geometry and areal density of the emission sites.[49] Constant A is 1.57×10^{-6} A eV/V^2, and constant B is 6.83 V/(eV$^{3/2}$ nm). We define the threshold electric field as the turn-on field (E_{to}) at J 10 μA/cm^2. These results are discussed below.

We select two sets of representative samples, with C_2H_2 flow rates of 11 and 2.7 sccm, to demonstrate the effects of the CNC growth time. For samples **18**, **20**, and **21** grown at 11 sccm, their EFE results are shown in Figure 8 and summarized in
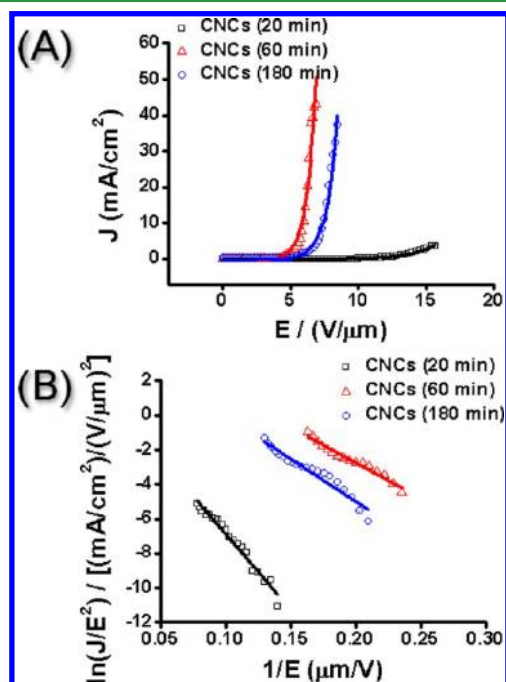

Figure 8. EFE properties of CNCs grown for different time lengths at 723 K and a C_2H_2 flow rate of 11 sccm. (A) $J−E$ curves and (B) FN plots. Samples **18**, **20**, and **21** were grown for 20, 60, and 180 min, respectively.

Table 1. Among them, sample **20** shows the best performance. Its E_{to}, β, and J at 5 V/μm are 3.78 V/μm, 1852, and 1.64 mA/cm^2, respectively. In addition, it can emit a high density of electrons of 43 mA cm^{-2} at a relatively low 6.87 V μm^{-1}. Sample **18** does not perform well because the CNC layer is relatively thin, as shown in Figure S7C in the Supporting Information. The CNCs in sample **21** are too crowded and wide in diameter, as shown in Figure S7G−I (Supporting Information). These probably cause a strong screening effect to

Table 1. Summary of Effects of Growth Time and Lengths on EFE Properties of CNCs at 723 K and a C_2H_2 Flow Rate of 11 sccm

sample	18	20	21
reaction time (min)	20	60	180
E_{to} (V/μm)	8.31	3.78	4.46
J (mA/cm^2) at 5 V/μm	1.73×10^{-4}	1.64	0.16
β	873	1852	1546

decrease the emission efficiency. In the cases of the flow rate 2.7 sccm, including samples **2**, **22**, and **23**, the results are shown in Figure S9 and Table S4 in the Supporting Information. For these samples, their EFE performances increase with increased growth time. The observation is attributed to increased aspect ratios and emission sites as the growth time was increased. All of the results discussed above suggest that the EFE properties could be optimized under a certain combination of CNC sizes and CNC layer thicknesses. In this investigation, when a C_2H_2 flow rate of 11 sccm was used to grow the CNCs, the products grew fast and long to result in better performances.

As discussed above, varying the carrier gas flowed into the reactor during the CVD affected the product morphology greatly. Also, it was found that H_2 was an essential component to assist the CNC formation. However, a concentration of H_2 restricted the CNC growths probably owing to the passivation of the K surface by hydrides. As shown in Figure S4 (Supporting Information), CNCs (sample **2**), curved NWs (sample **13**), and C particles (sample **14**) were grown by using H_2 (20 sccm), H_2 (30 sccm), and Ar (20 sccm), respectively. Their EFE results are shown in Figure S10 (Supporting Information) and summarized in Table S5 (Supporting Information). Among them, as expected, **14** does not emit electrons at the fields applied. Sample **2** performs much better than **13** does. Probably, **2**, with more curly bodies, provides more emission sites.[42] We also demonstrated that CNCs could be grown under a broad range of C_2H_2 concentrations. As shown in Figure 6, small diameter CNCs were synthesized at low flow rates of C_2H_2, while large diameter CNCs were grown at high concentrations of C_2H_2. Similar effects can be observed for the layer thicknesses of CNC layers. The EFE results of samples **2**, **17**, **18**, and **19** are shown in Figure S11 (Supporting Information) and summarized in Table S6 (Supporting Information). Among them, **19** presents the best performance. Probably, relatively large amounts of long CNCs in **19** provide a high density of electron emission sites and enhance the field

emission properties. The EFE measurements from three different sites on **19** show consistent results in Figure S12A in the Supporting Information. On the other hand, measuring two different samples of **20** (Figure S12B, Supporting Information) offers slightly different EFE performance. We expect the variations can be minimized by further process improvements.

■ CONCLUSIONS

In conclusion, we successfully synthesized CNCs with uniform morphology on bendable graphite substrates employing a Au and K bicatalyst assisted CVD process. The Au and K catalysts assisted the thermal decomposition of C_2H_2 to form CNCs cooperatively. The optimized CNC growth parameters were achieved by using Au NPs 30−37 nm, coating a K layer for 20 min (evaporated at 423 K), providing streams of C_2H_2 at 2.7−22 sccm and H_2 at 20 sccm, and setting the growth temperature at 723 K. By varying the growth time, the CNC lengths and the layer thicknesses could be controlled. The observations suggest that a tip-growth mechanism involving the Au NPs as the nucleation sites was in operation. In the reaction, the liquid-phase K metal assisted the decomposition of C_2H_2 by lowering the reaction temperature. We propose that acetylide and hydride intermediates were formed in the reaction. Further decomposition of the acetylide intermediates generated solid-phase C nucleated on the Au NPs and grown axially into NWs. The adhesion between the NW and the liquid-phase K particle would cause slower C atom deposition at the C−K interface, which is located at the inner curvature of the NW, than at the exposed C surface, the outer curvature. The phenomenon probably assists the NWs in curling into coils. Effects of varying the reaction conditions on the CNC growths are derived from the experimental data. They support the proposed bicatalyst enhanced tip-growth VLS mechanism. This is the second example of the bicatalyst system discovered so far.[13] For possible EFE applications, the best performed sample provided an E_{to} value of 3.78 V/μm and a field enhancement factor β of 1852. These are comparable to previously reported data summarized in Table 2. In addition, our sample revealed a current density, J, of 43 mA cm^{-2} at 6.87 V μm^{-1}. This is twice as much as the other reported values. Presumably, our high density and uniformly shaped CNCs allow the emission of high electron currents. Consequently, these low-temperature grown CNCs on bendable graphite substrates enable many possible flexible EFE device applications.

Table 2. Summary of Growth Parameters and EFE Characteristics of CNCs Reported in the Literature

nanomaterials	reaction gases (sccm)	growth/ annealing temp (K)	wire diameter/coil diameter/ pitch (nm)	carbon layer thickness (μm)	E_{to} (V/μm)	J_{max} (mA/cm^2)/E_{max} (V/μm)	β	ref
CNC on Cu tip	C_2H_2, 40/ NH_3, 100	873/−	−/200/−	100	1.3	11.17/2.39	2438−6430	50
CNC	C_2H_2, 60/ He, 300	973/−	−	−	1.3−2.62	−	−	51
crystalline CNC or CMC[a]	C_2H_2, 10 mbar	1023/−	−/120 − 1000/500	several	1.96−4.5	−	−	52
CNC	C_2H_2, 2.7/ H_2, 20	723/1423	80/100 − 300/100	ca. 75	2.51	17.71/5.64	2124	13
CNC	C_2H_2, 11/ H_2, 20	723/−	50−80/ 110−140/100−200	13−15	3.41−3.78	43/6.87	1852	this work

[a]Carbon microcoil: CMC.

■ ASSOCIATED CONTENT

Ⓢ Supporting Information

SEM images, tables, and figures of experimental data summaries. This material is available free of charge via the Internet at http://pubs.acs.org.

■ AUTHOR INFORMATION

Corresponding Author
*E-mail: htchiu@faculty.nctu.edu.tw.

Notes

The authors declare no competing financial interest.

■ ACKNOWLEDGMENTS

■ REFERENCES

(1) Coville, N. J.; Mhlanga, S. D.; Nxumalo, E. N.; Shaikjee, A. *S. Afr. J. Sci.* **2011**, *107*, 44−58.

(2) Chen, X.-Q.; Zhang, S.-L.; Dikin, D. A.; Ding, W.-Q.; Ruoff, R. S.; Pan, L.-J.; Nakayama, Y. *Nano Lett.* **2003**, *3*, 1299−1304.

(3) Antolini, E. *Appl. Catal., B* **2009**, *88*, 1−24.

(4) Che, J.-W.; Cagin, T.; Goddard, W. A. *Nanotechnology* **2000**, *11*, 65−69.

(5) Lin, C.-T.; Lee, C.-Y.; Chin, T.-S.; Xiang, R.; Ishikawa, K.; Shiomi, J.; Maruyama, S. *Carbon* **2011**, *49*, 1446−1452.

(6) Bower, C.; Zhu, W.; Shalom, D.; Lopez, D.; Chen, L.-H.; Gammel, P. L.; Jin, S. *Appl. Phys. Lett.* **2002**, *80*, 3820−3822.

(7) Koehne, J.; Chen, H.; Li, J.; Cassell, A. M.; Ye, Q.; Ng, H. T.; Han, J.; Meyyappan, M. *Nanotechnology* **2003**, *14*, 1239−1245.

(8) Choi, W. B.; Chu, J.-U.; Jeong, K.-S.; Bae, E.-J.; Lee, J.-W.; Kim, J.-J.; Lee, J.-O. *Appl. Phys. Lett.* **2001**, *79*, 3696−3698.

(9) Volodin, A.; Buntinx, D.; Ahlskog, M.; Fonseca, A.; Nagy, J. B.; Van Haesendonck, C. *Nano Lett.* **2004**, *4*, 1775−1779.

(10) Yang, S.; Chen, X.; Motojima, S. *Carbon* **2006**, *44*, 3352−3355.

(11) Wang, L.-S.; Buchholz, D. B.; Li, Y.; Li, J.; Lee, C.-Y.; Chiu, H.-T.; Chang, R. P. H. *Appl. Phys. A, Mater. Sci. Process.* **2007**, *87*, 1−6.

(12) Jeong, H.-J.; Jeong, H.-D.; Kim, H.-Y.; Kim, J.-S.; Jeong, S.-Y.; Han, J.-T.; Bang, D.-S.; Lee, G.-W. *Adv. Funct. Mater.* **2011**, *21*, 1526−1532.

(13) Liu, W.-C.; Lin, H.-K.; Chen, Y.-L.; Lee, C.-Y.; Chiu, H.-T. *ACS Nano* **2010**, *4*, 4149−4157.

(14) Venkatesan, N.; Yoshimitsu, J.; Ito, Y.; Shibata, N.; Takada, K. *Biomaterials* **2005**, *26*, 7154−7163.

(15) Klumpp, C.; Kostarelos, K.; Prato, M.; Bianco, A. *Biochim. Biophys. Acta-Biomembr.* **2006**, *1758*, 404−412.

(16) Jiang, F.; Wang, S.; Lin, J.-J.; Jin, H.-L.; Zhang, L.-J.; Huang, S.-M.; Wang, J.-C. *Electrochem. Commun.* **2011**, *13*, 363−365.

(17) Chang, J.-C.; Tzeng, Y.-F.; Chen, J.-M.; Chiu, H.-T.; Lee, C.-Y. *Electrochim. Acta* **2009**, *54*, 7066−7070.

(18) Hyeon, T.; Han, S.; Sung, Y.-E.; Park, K.-W.; Kim, Y.-W. *Angew. Chem., Int. Ed.* **2003**, *42*, 4352−4356.

(19) Chen, W.-Y.; Wang, L.-S.; Chiu, H.-T.; Chen, Y.-C.; Lee, C.-Y. *J. Am. Soc. Mass Spectrom.* **2004**, *15*, 1629−1635.

(20) Zhang, L.; Zhu, Y.-B.; Ge, C.-L.; Wei, C.; Wang, Q.-L. *Solid State Commun.* **2007**, *142*, 541−544.

(21) Lanjuan, W.; Chunzhong, L.; Feng, G.; Chuanxiang, Z. *J. Alloys Compd.* **2009**, *473*, 351−355.

(22) Sevilla, M.; Sanchís, C.; Valdés-Solís, T.; Morallón, E.; Fuertes, A. B. *Electrochim. Acta* **2009**, *54*, 2234−2238.

(23) Qi, X.-S.; Zhong, W.; Deng, Y.; Au, C.-T.; Du, Y.-W. *Carbon* **2010**, *48*, 365−376.

(24) Tang, N.; Zhong, W.; Au, C.; Yang, Y.; Han, M.; Lin, K.; Du, Y. *J. Phys. Chem. C* **2008**, *112*, 19316−19323.

(25) Jian, X. A.; Jiang, M.; Zhou, Z. W.; Yang, M.-L.; Lu, J.; Hu, S.-C.; Wang, Y.; Hui, D. *Carbon* **2010**, *48*, 4535−4541.

(26) Nitze, F.; Abou-Hamad, E.; Wagberg, T. *Carbon* **2011**, *49*, 1101−1107.

(27) Neng-Kai, C.; Shuo-Hung, C. *Carbon* **2008**, *46*, 1106−1109.

(28) Yang, S.; Chen, X.; Kikuchi, N.; Motojima, S. *Mater. Lett.* **2008**, *62*, 1462−1465.

(29) Kawaguchi, M.; Nozaki, K.; Motojima, S.; Iwanaga, H. *J. Cryst. Growth* **1992**, *118*, 309−313.

(30) In-Hwang, W.; Chen, X. Q.; Kuzuya, T.; Kawabe, K.; Motojima, S. *Carbon* **2000**, *38*, 565−571.

(31) Amelinckx, S.; Zhang, X.-B.; Bernaerts, D.; Zhang, X.-F.; Ivanov, V.; Nagy, J. B. *Science* **1994**, *265*, 635−639.

(32) Bandaru, P. R.; Daraio, C.; Yang, K.; Rao, A.-M. *J. Appl. Phys.* **2007**, *101*, 094307−4.

(33) Fang, X.-S.; Bando, Y.; Gautam, U. K.; Ye, C.; Golberg, D. *J. Mater. Chem.* **2008**, *18*, 509−522.

(34) Wu, H.-C.; Tsai, H.-Y.; Chiu, H.-T.; Lee, C.-Y. *ACS Appl. Mater. Interfaces* **2010**, *2*, 3285−3288.

(35) Wu, H.-C.; Tsai, T.-Y.; Chu, F.-H.; Tai, N.-H.; Lin, H.-N.; Chiu, H.-T.; Lee, C.-Y. *J. Phys. Chem. C* **2010**, *114*, 130−133.

(36) Wu, H.-C.; Hou, T.-C.; Chueh, Y.-L.; Chen, L.-J.; Chiu, H.-T.; Lee, C.-Y. *Nanotechnology* **2010**, *21*, 455601−4.

(37) Chang, I.-C.; Huang, T.-K.; Lin, H.-K.; Tzeng, Y.-F.; Peng, C.-W.; Pan, F.-M.; Lee, C.-Y.; Chiu, H.-T. *ACS Appl. Mater. Interfaces* **2009**, *1*, 1375−1378.

(38) Zhao, Q.; Gao, J.-Y.; Zhu, R.; Cai, T.-C.; Wang, S.; Song, X.-F.; Liao, Z.-M.; Chen, X.-H.; Yu, D.-P. *Nanotechnology* **2010**, *21*, 095701−6.

(39) Tseng, Y.-K.; Huang, C.-J.; Cheng, H.-M.; Lin, I.-N.; Liu, K.-S.; Chen, I.-C. *Adv. Funct. Mater.* **2003**, *13*, 811−814.

(40) Hsieh, C.-T.; Chen, J.-M.; Lin, H.-H.; Shih, H.-C. *Appl. Phys. Lett.* **2003**, *83*, 3383−3385.

(41) Lin, H.-K.; Tzeng, Y.-F.; Wang, C.-H.; Tai, N.-H.; Lin, I.-N.; Lee, C.-Y.; Chiu, H.-T. *Chem. Mater.* **2008**, *20*, 2429−2431.

(42) Pan, L.; Konishi, O.; Tanaka, H.; Suekane, O.; Nosaka, T.; Nakayama, Y. *Jpn. J. Appl. Phys. Part 1 - Regul. Pap. Brief Commun. Rev. Pap.* **2005**, *44*, 1652−1654.

(43) Agarwal, S.; Sarada, B. Y.; Kar, K. K. *Nanotechnology* **2010**, *21*, 65601−5.

(44) Wang, L.-S. Ph.D. Thesis, National Chiao Tung University, 2006.

(45) Takagi, D.; Homma, Y.; Hibino, H.; Suzuki, S.; Kobayashi, Y. *Nano Lett.* **2006**, *6*, 2462−2465.

(46) Yuan, D. N.; Ding, L.; Chu, H. B.; Feng, Y. Y.; McNicholas, T. P.; Liu, J. *Nano Lett.* **2008**, *8*, 2576−2579.

(47) Kuzuya, C.; In-Hwang, W.; Hirako, S.; Hishikawa, Y.; Motojima, S. *Chem. Vapor Deposition* **2002**, *8*, 57−62.

(48) Okamoto, H.; Massalski, T. *J. Phase Equilib.* **1984**, *5*, 378−379.

(49) Bonard, J. M.; Weiss, N.; Kind, H.; Stöckli, T.; Forró, L.; Kern, K.; Châtelain, A. *Adv. Mater.* **2001**, *13*, 184−188.

(50) Sung, W.-Y.; Ok, J. G.; Kim, W.-J.; Lee, S.-M.; Yeon, S.-C.; Lee, H.-Y.; Kim, Y.-H. *Nanotechnology* **2007**, *18*, 245603−5.

(51) Pan, L.-J.; Hayashida, T.; Zhang, M.; Nakayama, Y. *Jpn. J. Appl. Phys. Part 2 - Lett.* **2001**, *40*, L235−L237.

(52) Banerjee, D.; Jha, A.; Chattopadhyay, K. K. *Appl. Surf. Sci.* **2010**, *256*, 7516−7521.